A. Attachments

A.1 List of publications

List of publications

First-authored publications

[A1] M. Imrisek, V. Weinzettl, J. Mlynar, T. Odstrcil, M. Odstrcil, O. Ficker, J. R. Pinzon, C. Ehrlacher, R. Panek, M. Hron, and et al. Use of soft x-ray diagnostic on the compass tokamak for investigations of sawteeth crash neighborhood and of plasma position using fast inversion methods. *Review of Scientific Instruments*, 85(11), 2014.

[A2] M. Imríšek, J. Mlynář, V. Löffelmann, V. Weinzettl, T. Odstrčil, M. Odstrčil, and M. Tomeš. Optimization of soft x-ray tomography on the compass tokamak. *Nukleonika*, 61(4):403–408, 2016.

Co-authored publications related to the thesis

[B1] J. Mlynar, M. Imrisek, V. Weinzettl, M. Odstrcil, J. Havlicek, F. Janky, B. Alper, and A. Murari. Introducing minimum fisher regularisation tomography to axuv and soft x-ray diagnostic systems of the compass tokamak. *Review of Scientific Instruments*, 83(10), 2012.

[B2] J. Mlynar, D. Mazon, M. Imrisek, V. Loffelmann, P. Malard, T. Odstrcil, M. Tomes, D. Vezinet, and V. Weinzettl. Soft x-ray tomography in support of impurity control in tokamaks. *Journal of Physics: Conference Series*, 768:012001, 2016.

[B3] R. Pánek et al. Status of the COMPASS tokamak and characterization of the first h-mode. *Plasma Physics and Controlled Fusion*, 58(1):014015, October 2015.

[B4] J. Mlynar, M. Tomes, M. Imrisek, B. Alper, Ma. O'Mullane, T. Odstrcil, and T. Puetterich. Soft x-ray tomographic reconstruction of jet ilw plasmas with tungsten impurity and different spectral response of detectors. *Fusion Engineering and Design*, 96-97:869–872, 2015.

[B5] V. Loffelmann, J. Mlynar, M. Imrisek, D. Mazon, A. Jardin, V. Weinzettl, and M. Hron. Minimum fisher tikhonov regularization adapted to real-time tomography. *Fusion Science and Technology*, 69(2):505–513, 2016.

[B6] J. Horacek, G. Cunningham, S. Entler, P. Dobias, R. Duban, M. Imrisek, T. Markovic, J. Havlicek, and R. Enikeev. Feasibility study of fast swept divertor strike point suppressing transient heat fluxes in big tokamaks. *Fusion Engineering and Design*, 123:646–649, 2017.

[B7] R. Panek, T. Markovic, P. Cahyna, R. Dejarnac, J. Havlicek, J. Horacek, M. Hron, M. Imrisek, P. Junek, M. Komm, and et al. Conceptual design of the compass upgrade tokamak. *Fusion Engineering and Design*, 123:11–16, 2017.

[B8] J. Mlynar, T. Craciunescu, D. R. Ferreira, P. Carvalho, O. Ficker, O. Grover, M. Imrisek, and J. Svoboda. Current research into applications of tomography for fusion diagnostics. *Journal of Fusion Energy*, 38(3-4):458–466, 2018.

[B9] M. Komm, I. Khodunov, J. Cavalier, P. Vondracek, S. Henderson, J. Seidl, J. Horacek, D. Naydenkova, J. Adamek, P. Bilkova, and et al. Divertor impurity seeding experiments at the compass tokamak. *Nuclear Fusion*, 59(10):106035, 2019.

[B10] M Komm, D Mancini, M Morbey, J Cavalier, J Adamek, M Bernert, P Bilkova, P Bohm, D Brida, O Février, et al. Power exhaust by core radiation at compass tokamak. *Nuclear Fusion*, 61(3):036016, 2021.

[B11] P Vondracek, R Panek, M Hron, J Havlicek, V Weinzettl, T Todd, D Tskhakaya, G Cunningham, P Hacek, J Hromadka, et al. Preliminary design of the compass upgrade tokamak. *Fusion Engineering and Design*, 169:112490, 2021.

[B12] Martin Hron, Jiri Adamek, Jordan Cavalier, Renaud Dejarnac, Ondřej Ficker, Ondrej Grover, Jan Horacek, Michael Komm, Eva Macusova, Ekaterina Matveeva, et al. Overview of the compass results. *Nuclear Fusion*, 2021.

Co-authored proceedings related to the thesis

[C1] M. Imríšek, J. Havlíček, V. Weinzettl, and J. Mlynář. Observation of sawtooth oscillations in the compass tokamak. pages 67–72. MATFYZPRESS, 2013.

[C2] R. Pánek, J. Stöckel, J. Havlíček, F. Janky, M. Hron, V. Weinzettl, P. Bílková, M. Dimitrova, Dejarnac R. Háček, P., M. Aftanas, P. Böhm, P. Cahyna, M. Imríšek, E. Štefániková, and J. Varju. Characterization of ohmic and nbi heated h-mode in the compass tokamak. pages P4.103–P4.103. European Physical Society, 2013.

[C3] M. Komm, J. Cavalier, J. Seidl, J. Adámek, P. Bílková, P. Böhm, A. Devitre, M. Dimitrova, S. Elmore, M. Faitsch, P. Háček, J. Havlíček, M. Imríšek, J. Krbec, M. Peterka, R. Pánek, T. Popov, M. Tomeš, and V. Weinzettl. First detachment studies on compass tokamak using nitrogen seeding. In E.; Riconda C.; Melzer A.; Bret A.; Dromey B. Fajardo, M.; Westerhof, editor, *Proceedings of 44th European Physical Society Conference on Plasma Physics*, volume 41F, page P5.005. European Physical Society, 2017.

Other co-authored publications

[D1] P. Ivanova, M. Dimitrova, E. Vasileva, Tsv. K. Popov, R. Dejarnac, J. Stockel, M. Imrisek, P. Hacek, and R. Panek. Determination of the plasma potential and the eedf by langmuir probes in the divertor region of compass tokamak. *Journal of Physics: Conference Series*, 768:012003, 2016.

[D2] F. Romanelli. Overview of the jet results. *Nuclear Fusion*, 55(10):104001, 2015.

[D3] V. Weinzettl, G. Shukla, J. Ghosh, R. Melich, R. Panek, M. Tomes, M. Imrisek, D. Naydenkova, J. Varju, T. Pereira, and et al. High-resolution spectroscopy diagnostics for measuring impurity ion temperature and velocity on the compass tokamak. *Fusion Engineering and Design*, 96-97:1006–1011, 2015.

[D4] M. Vlainić, P. Vondráček, J. Mlynář, V. Weinzettl, O. Ficker, M. Varavin, R. Papřok, M. Imríšek, J. Havlíček, R. Pánek, and J.-M. Noterdaeme. Synchrotron radiation from runaway electrons in compass tokamak. volume 39E, page P4.108. European Physical Society, 2015.

[D5] J. Horacek, P. Vondracek, R. Panek, R. Dejarnac, M. Komm, R.a. Pitts, M. Kocan, R.j. Goldston, P.c. Stangeby, E. Gauthier, and et al. Narrow heat flux channels in the compass limiter scrape-off layer. *Journal of Nuclear Materials*, 463:385–388, 2015.

[D6] A. V. Melnikov, T. Markovic, L. G. Eliseev, J. Adámek, M. Aftanas, P. Bilkova, P. Boehm, M. Gryaznevich, M. Imrisek, S. E. Lysenko, and et al. Quasicoherent modes on the compass tokamak. *Plasma Physics and Controlled Fusion*, 57(6):065006, 2015.

[D7] M. Vlainić, J. Mlynář, V. Weinzettl, R. Papřok, M. Imríšek, O. Ficker, P. Vondráček, and J. Havlíček. First dedicated observations of runaway electrons in the compass tokamak. *Nukleonika*, 60(2):249–255, 2015.

[D8] M. Vlainic, J. Mlynar, J. Cavalier, V. Weinzettl, R. Paprok, M. Imrisek, O. Ficker, M. Varavin, P. Vondracek, J.-M. Noterdaeme, and et al. Post-disruptive runaway electron beams in the compass tokamak. *Journal of Plasma Physics*, 81(5), 2015.

[D9] T. Markovic, Y.q. Liu, P. Cahyna, R. Pánek, M. Peterka, M. Aftanas, P. Bílková, P. Bohm, M. Imríšek, P. Háček, and et al. Measurements and modelling of plasma response field to rmp on the compass tokamak. *Nuclear Fusion*, 56(9):092010, 2016.

[D10] M. Tomeš, V. Weinzettl, T. Pereira, M. Imríšek, and J. Seidl. Calculation of edge ion temperature and poloidal rotation velocity from carbon iii triplet measurements on the compass tokamak. *Nukleonika*, 61(4):443–451, 2016.

[D11] O. Ficker, J. Mlynar, M. Vlainic, J. Cerovsky, J. Urban, P. Vondracek, V. Weinzettl, E. Macusova, J. Decker, M. Gospodarczyk, and et al. Losses of runaway electrons in mhd-active plasmas of the compass tokamak. *Nuclear Fusion*, 57(7):076002, 2017.

[D12] M. Dimitrova, Tsv. K. Popov, J. Adamek, J. Kovačič, P. Ivanova, E. Hasan, D. López-Bruna, J. Seidl, P. Vondráček, R. Dejarnac, and et al. Plasma potential and electron temperature evaluated by ball-pen and langmuir probes in the compass tokamak. *Plasma Physics and Controlled Fusion*, 59(12):125001, 2017.

[D13] H. Meyer et al. Overview of progress in european medium sized tokamaks towards an integrated plasma-edge/wall solution. *Nuclear Fusion*, 57(10):102014, June 2017.

[D14] V. Weinzettl, J. Matejicek, S. Ratynskaia, P. Tolias, M. De Angeli, G. Riva, M. Dimitrova, J. Havlicek, J. Adamek, J. Seidl, and et al. Dust remobilization experiments on the compass tokamak. *Fusion Engineering and Design*, 124:446–449, 2017.

[D15] J. Seidl, J. Krbec, M. Hron, J. Adamek, C. Hidalgo, T. Markovic, A.v. Melnikov, J. Stockel, V. Weinzettl, M. Aftanas, and et al. Electromagnetic characteristics of geodesic acoustic mode in the compass tokamak. *Nuclear Fusion*, 57(12):126048, 2017.

[D16] P. Vondracek, E. Gauthier, O. Ficker, M. Hron, M. Imrisek, and R. Panek. Fast infrared thermography on the compass tokamak. *Fusion Engineering and Design*, 123:764–767, 2017.

[D17] T. Jirman, M. Peterka, J. Seidl, J. Cavalier, V. Weinzettl, F. Brochard, P. Cahyna, J. Harrison, M. Imrisek, A. Kirk, and et al. Edge plasma study using a fast visible light camera in the compass tokamak. *Energy Procedia*, 127:360–368, 2017.

[D18] Komm M., Cavalier J., Seidl J., Adámek J., Bílková P., Böhm P., Devitre A., Dimitrova M., Elmore S., Faitsch M., Háček P., Havlíček J., Imríšek M., Krbec J., Peterka M., Pánek R., Popov T., Tomeš M., and Weinzettl V. First detachment studies on compass tokamak using nitrogen seeding. In E.; Riconda C.; Melzer A.; Bret A.; Dromey B. Fajardo, M.; Westerhof, editor, *Proceedings of 44th European Physical Society Conference on Plasma Physics*, volume 41F, page P5.005. European Physical Society, 2017.

[D19] X. Litaudon, S. Abduallev, M Abhangi, P. Abreu, M. Afzal, K. M. Aggarwal, T. Ahlgren, Jong Hyun Ahn, L. Aho-Mantila, N. Aiba, et al. Overview of the jet results in support to iter. *Nuclear Fusion*, 57(10):102001, 2017.

[D20] V.v. Plyusnin, C. Reux, V.g. Kiptily, G. Pautasso, J. Decker, G. Papp, A. Kallenbach, V. Weinzettl, J. Mlynar, S. Coda, and et al. Comparison of runaway electron generation parameters in small, medium-sized and large tokamaks—a survey of experiments in compass, tcv, asdex-upgrade and jet. *Nuclear Fusion*, 58(1):016014, 2017.

[D21] D.d. Carvalho, D. R. Ferreira, P. J. Carvalho, M. Imrisek, J. Mlynar, H. Fernandes, and Jet Contributors. Deep neural networks for plasma tomography with applications to jet and compass. *Journal of Instrumentation*, 14(09), 2019.

[D22] V.v. Yanovskiy, N. Isernia, V.d. Pustovitov, F. Villone, D. Abate, P. Bettini, S. L. Chen, J. Havlicek, A. Herrmann, J. Hromadka, and et al. Comparison of approaches to the electromagnetic analysis of compass-u vacuum vessel during fast transients. *Fusion Engineering and Design*, 146:2338–2342, 2019.

[D23] S. Brezinsek, A. Kirschner, M. Mayer, A. Baron-Wiechec, I. Borodkina, D. Borodin, I. Coffey, J. Coenen, N. Den Harder, A. Eksaeva, and et al. Erosion, screening, and migration of tungsten in the jet divertor. *Nuclear Fusion*, 59(9):096035, 2019.

[D24] M. Varavin, A. Varavin, D. Naydenkova, J. Zajac, F. Zacek, S. Nanobashvili, R. Panek, V. Weinzettl, P. Bilkova, K. Kovarik, and et al. Study for the microwave interferometer for high densities plasmas on compass-u tokamak. *Fusion Engineering and Design*, 146:1858–1862, 2019.

[D25] J. Mlynar, O. Ficker, E. Macusova, T. Markovic, D. Naydenkova, G. Papp, J. Urban, M. Vlainic, P. Vondracek, V. Weinzettl, and et al. Runaway electron experiments at compass in support of the eurofusion iter physics research. *Plasma Physics and Controlled Fusion*, 61(1):014010, 2018.

[D26] O. Ficker, E. Macusova, J. Mlynar, D. Bren, A. Casolari, J. Cerovsky, M. Fárník, O. Grover, J. Havlicek, A. Havranek, et al. Runaway electron beam stability and decay in compass. *Nuclear Fusion*, 59(9):096036, 2019.

[D27] V. Weinzettl, J. Adamek, P. Bilkova, J. Havlicek, R. Panek, M. Hron, O. Bogar, P. Bohm, A. Casolari, J. Cavalier, and et al. Constraints on conceptual design of diagnostics for the high magnetic field compass-u tokamak with hot walls. *Fusion Engineering and Design*, 146:1703–1707, 2019.

[D28] P. Wachal, J. Błocki, J. Hromádka, P. Háček, D. Šesták, J. Havlíček, P. Junek, M. Imríšek, L. Kripner, M. Peterka, and et al. Development and mechanical investigation of central solenoid structure for compass-u tokamak. *3Rd National Conference On Current And Emerging Process Technologies – Concept 2020*, 2020.

[D29] Emmanuel Joffrin, Sadrilla Abduallev, Mitul Abhangi, P Abreu, V Afanasev, M Afzal, KM Aggarwal, T Ahlgren, L Aho-Mantila, N Aiba, et al. Overview of the jet preparation for deuterium–tritium operation with the iter like-wall. *Nuclear Fusion*, 59(11):112021, 2019.

[D30] M. Dimitrova, Tsv. K. Popov, J. Kovacic, R. Dejarnac, J. P. Gunn, P. Ivanova, M. Imrisek, J. Stöckel, P. Vondracek, M. Hron, and et al. Impact of impurity seeding on the electron energy distribution function in the compass divertor region. *Plasma Physics and Controlled Fusion*, 62(12):125015, 2020.

[D31] K. Mikszuta-Michalik, M. Imrisek, B. Esposito, D. Marocco, J. Mlynar, and O. Ficker. A total neutron yield constraint implemented to the rnc emissivity reconstruction on iter tokamak. *Fusion Engineering and Design*, 160:111840, 2020.

[D32] R. Dejarnac, J. Horacek, M. Hron, M. Jerab, J. Adamek, S. Atikukke, P. Barton, J. Cavalier, J. Cecrdle, M. Dimitrova, and et al. Overview of power exhaust experiments in the compass divertor with liquid metals. *Nuclear Materials and Energy*, 25:100801, 2020.

[D33] N. Patel, J. Hromadka, D. Sestak, J. Havlicek, V. Balner, V. Veselovsky, K. Samec, M. Hron, R. Panek, V. Yanovskiy, and et al. Design study of vacuum vessel concepts for compass-u tokamak. *IEEE Transactions on Plasma Science*, 48(6):1452–1456, 2020.

[D34] Sara Moradi, Johan Anderson, Michele Romanelli, Hyun-Tae Kim, X Litaudon, S Abduallev, M Abhangi, P Abreu, M Afzal, KM Aggarwal, et al. Global scaling of the heat transport in fusion plasmas. *Physical Review Research*, 2(1):013027, 2020.

[D35] F Jaulmes, G Zadvitskiy, K Bogar, M Imrisek, J Hromadka, SY Cats, J Varju, M Komm, and R Panek. Modelling of charge-exchange induced nbi losses in the compass upgrade tokamak. *Nuclear Fusion*, 61(4):046012, 2021.

[D36] I Khodunov, M Komm, A Havranek, J Adamek, P Bohm, J Cavalier, J Seidl, A Devitre, M Dimitrova, S Elmore, et al. Real-time feedback system for divertor heat flux control at compass tokamak. *Plasma Physics and Controlled Fusion*, 63(6):065012, 2021.

[D37] Jakub Hromadka, Josef Havlicek, Nisarg Patel, Vadim Yanovskiy, Karel Patocka, Jan Prevratil, Martin Imrisek, Fabien Jaulmes, Arthur Brooks, Peter Titus, et al. Electromagnetic model for finite element analyses of plasma disruption events used in the design phase of the compass-u tokamak. *Fusion Engineering and Design*, 167:112369, 2021.

[D38] J Horacek, J Cecrdle, D Tskhakaya, R Dejarnac, J Schwartz, M Komm, J Cavalier, J Adamek, S Lukes, V Veselovsky, et al. Predictive modelling of liquid metal divertor: from compass tokamak towards upgrade. *Physica Scripta*, 96(12):124013, 2021.

[D39] Matej Tomes, Matthew Carr, Alex Meakins, Martin Imrisek, Fabien Jaulmes, Vojtech Balner, Klara Bogar, Petra Bilkova, Vladimir Weinzettl, Martin Hron, et al. Feasibility study and cxrs synthetic diagnostic model for compass upgrade based on cherab and raysect framework. *Fusion Engineering and Design*, 170:112498, 2021.

Other co-authored proceedings

[E1] D. Naydenkova, V. Weinzettl, J. Stöckel, P. Háček, and M. Imríšek. Absolute sensitivity calibration of visible spectroscopic diagnostic and temporal evolution of first window transmittance at the compass tokamak. pages 97–103. MATFYZPRESS, 2013.

[E2] V. Weinzettl, M. Imríšek, J. Havlíček, L. Kripner, J. Seidl, P. Bílková, P. Böhm, M. Aftanas, K. Kovařík, J. Horáček, P. Vondráček, J. Adámek, R. Dejarnac, and D. Cornelis. Experimental evidence of neoclassical tearing modes on compass tokamak. pages P4.103–P4.103. European Physical Society, 2013.

[E3] J. Havlíček, M. Imríšek, K. Kovařík, and V. Weinzettl. Global power balance in non-stationary discharge phases in the compass tokamak. pages 204–210. MATFYZPRESS, 2014.

[E4] T. Markovič, J. Seidl, A. Melnikov, P. Háček, J. Havlíček, A. Havránek, M. Hron, O. Hronová-Bilyková, M. Imríšek, F. Janky, K. Kovařík, O. Mikulín, R. Pánek, R. Papřok, J. Pipek, P. Vondráček, and V. Weinzettl. Alfvén-wave character oscillations in tokamak compass plasma. page P4.104. European Physical Society, 2015.

[E5] J. Seidl, M. Hron, J. Adámek, P. Vondráček, J. Horáček, C. Hidalgo, A. Melnikov, L. Eliseev, T. Markovič, J. Stöckel, D. Basu, P. Háček, J. Havlíček, M. Imríšek, K. Kovařík, l V. Weinzett, and R. Pánek. Observation of geodesic acoustic mode-like oscillations on compass. volume 39E, page P4.103. European Physical Society, 2015.

[E6] M. Vlainić, J. Mlynář, V. Weinzettl, R. Papřok, M. Imríšek, O. Ficker, P. Vondráček, and J. Havlíček. First dedicated observations of runaway electrons in the compass tokamak. *Nukleonika*, 60(2):249–255, 2015.

[E7] O. Ficker, J. Mlynar, M. Vlainic, J. Cerovsky, J. Urban, P. Vondracek, V. Weinzettl, E. Macusova, J. Decker, M. Gospodarczyk, and et al. Losses of runaway electrons in mhd-active plasmas of the compass tokamak. *Nuclear Fusion*, 57(7):076002, 2017.

[E8] Markovič T., Melnikov A., Seidl J., Eliseev L., Havlíček J., Havránek A., Hron M., Imríšek M., Kovařík K., Medvedev S., Mitošinková K., Mlynář J., Naydenkova D., Pánek R., Stöckel J., Varju J., and Weinzettl V. Observations of alfvénic-character oscillations in ohmic plasmas on the compass tokamak. In E.; Riconda C.; Melzer A.; Bret A.; Dromey B. Fajardo, M.; Westerhof, editor, *Proceedings of 44th European Physical Society Conference on Plasma Physics*, volume 41F, page P5.005. European Physical Society, 2017.

[E9] P Bílková, P Böhm, M Komm, Lorenzo Frassinetti, E Štefániková, M Peterka, M Šos, J Seidl, O Grover, J Havlíček, et al. Relative shift in position of temperature and density pedestals at the compass tokamak. In *44th European Physical Society Conference on Plasma Physics, EPS 2017, 26 June 2017 through 30 June 2017*. European Physical Society (EPS), 2017.

[E10] T Markovic, A Melnikov, J Seidl, L Eliseev, J Havlicek, A Havránek, M Hron, M Imríšek, K Kovarík, S Medvedev, et al. Observations of alfvénic-character oscillations in ohmic plasmas on the compass tokamak. In *Proc. 43rd EPS Conf. on Plasma Physics (Leuven, Belgium, 4–8 July 2016)*, 2016.

[E11] T Markovic, A Melnikov, J Seidl, L Eliseev, J Havlicek, A Havránek, M Hron, M Imríšek, and K Kovarík. Alfvén-character oscillations in ohmic plasmas observed on the compass tokamak. In *Proc. 44th EPS Conf. Plasma Physics*, pages 26–30, 2017.

[E12] J Urban, A Casolari, D Fridrich, F Jaulmes, J Havlicek, M Hron, M Imrisek, M Komm, L Kripner, E Macusova, et al. Performance predictions for the compass upgrade tokamak. volume 42A, pages 121–124. European Physical Society, 2018.

[E13] O Ficker, M Imrisek, J Mlynar, E Macusova, J Svoboda, V Weinzettl, J Urban, A Havranek, J Cerovsky, M Farnik, et al. Analysis of mgi disruptions and runaway electron beams at compass using tomography and fast camera data. In *45th EPS Conference on Plasma Physics, Prague, Czech Republic*, volume 42A, pages 353–356. European Physical Society, 2018.

[E14] Markovič T., Peterka M., Loarte A., Park K., Gribov Y., Pánek R., Háček P., Havlíček J., Hron M., Imríšek M., Kovařík K., Kripner L., Bogár K., Šos M., Tomeš M., Varju J., Vondráček P., and Weinzettl V. High-field side error field effects on h-mode plasma performance and their correction in iter-like experiments on compass. In *45th EPS Conference on Plasma Physics, Prague, Czech Republic*. European Physical Society, 2018.

A.2 Attached article: Optimization of soft X-ray tomography on the COMPASS tokamak

Optimization of soft X-ray tomography on the COMPASS tokamak

Martin Imríšek,
Jan Mlynář,
Viktor Löffelmann,
Vladimír Weinzettl,
Tomáš Odstrčil,
Michal Odstrčil,
Matěj Tomeš

Abstract. The COMPASS tokamak is equipped with the soft X-ray (SXR) diagnostic system based on silicon photodiode arrays shielded by a thin beryllium foil. The diagnostic is composed of two pinhole cameras having 35 channels each and one vertical pinhole camera with 20 channels, which was installed recently to improve tomographic inversions. Lines of sight of the SXR detectors cover almost complete poloidal cross section of the COMPASS vessel with a spatial resolution of 1–2 cm and temporal resolution of about 3 μs. Local emissivity is reconstructed via Tikhonov regularization constrained by minimum Fisher information that provides reliable and robust solution despite limited number of projections and ill-conditionality of this task. Improved border conditions and numerical differentiation matrices suppressing artifacts in reconstructed radiation were implemented in the code. Furthermore, a fast algorithm eliminating iterative processes was developed, and it is foreseen to be tested in real-time plasma control.

Key words: soft X-ray • tomography • Tikhonov regularization • tokamak

M. Imríšek✉ J. Mlynář, V. Löffelmann, V. Weinzettl,
M. Tomeš
Institute of Plasma Physics ASCR v.v.i.,
Faculty of Mathematics and Physics,
Charles University in Prague,
Za Slovankou 3, 18200 Praha 8, Czech Republic,
Tel.: +42 060 381 0107,
E-mail: imrisek@ipp.cas.cz

T. Odstrčil
Max-Planck-Institut für Plasmaphysik,
Technische Universität Munchen,
Boltzmannstraße 2, D-85748 Garching, Germany

M. Odstrčil
Optoelectronic Research Center,
University of Southampton,
University Rd, Southampton SO17 1BJ, United Kingdom

Introduction

In tokamak plasmas, soft X-ray (SXR) radiation represents a useful quantity for diagnostics of various processes in plasma core. SXR radiation power is given predominantly by bremsstrahlung and line radiation of heavy impurities (tungsten, iron). Bremsstrahlung is generated mainly by the elastic electron-ion collisions (in the nonrelativistic limit, radiation fields produced by two particles in like-particle collision cancel) and the SXR-radiated power density is, therefore, dependent on electron density n_e, density of Z_j-times charged ion species n_j, and electron temperature T_e:

$$(1) \qquad P_{brem} \propto \sum z_j n_j n_e \sqrt{T_e}$$

Line radiation is emitted by bound-bound transitions of excited electrons in atoms and non-fully ionized ions. In the case of negligible particle transport, intensity of the line radiation from specific location is proportional to the density of ion species, electrons, and it is also a function of electron temperature, as collisions with free electrons excite bound electrons. In tokamaks, SXR line radiation is generated by heavy impurities such as tungsten or iron, which can contaminate plasma because of plasma wall interactions. Impurity accumulation has a serious impact on the tokamak performance, as it results in a cooling of plasma and a dilution of the hydrogen isotopes (i.e., reduction of possible fusion reactions rate).

The character of mechanisms generating the SXR radiation makes its measurement suitable for monitoring plasma processes connected with perturbation of density and temperature (sawtooth instability, magnetohydrodynamic (MHD) modes) and monitoring impurity profiles with high temporal and spatial resolution. Moreover, SXR measurements can provide information on plasma position and shape.

Soft X-ray diagnostic on the COMPASS tokamak

The COMPASS tokamak is a divertor device with clear H-mode and ITER-relevant geometry (1:10 to ITER plasma size, $R = 0.56$ m, $a = 0.23$ m, $I_p < 400$ kA, $B_T \sim 1.15$ T, and a typical pulse length of about 300 ms) [1]. Limiter and divertor tiles are made of graphite. Therefore, the concentration of heavy impurities in plasma is low and the main source of the SXR radiation is bremsstrahlung.

The current SXR diagnostic system at COMPASS consists of three pinhole cameras. Each camera has one photodiode array shielded by a 10-μm thick beryllium foil. The system contains two arrays of 35 detectors (type LD35-5T) and one array of 20 detectors [2] (IRD, type AXUV-20EL) covering almost the whole poloidal cross section (see Fig. 1 and Fig. 2). The spectral sensitivity (shown in Fig. 3) is given mainly by the thickness of the beryllium foil blocking low energy photons (below 1 keV) and by the diode active layer, which is 200 μm thick. Temporal resolution is limited mainly by the amplifier to 3 μs, allowing investigation of fast MHD processes such as internal kink modes (with frequency of about 40 kHz) or sawtooth oscillations (about 500 Hz). The spatial resolution of each camera is 1–2 cm.

Tomographic reconstruction

Tomography allows reconstructing local parameters from line-integrated measurements. Its solution can be found either analytically by transformation
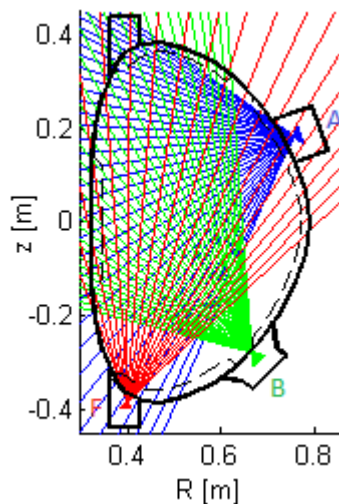

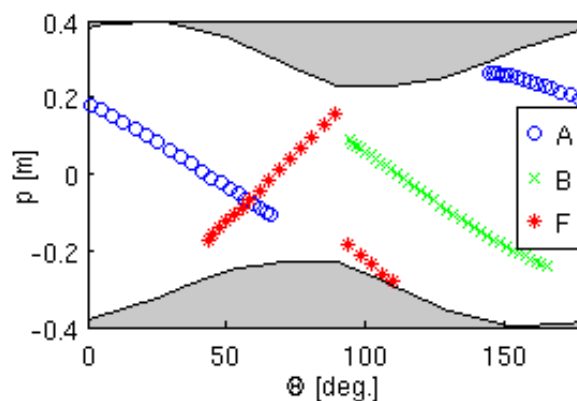**Fig. 1.** Lines of sight of the SXR detectors on the COMPASS tokamak.

Fig. 2. Coverage in projection space where *p* is the distance from the center of chamber and Θ angle with respect to the horizontal axis.

methods or by series expansion methods searching for a solution given as a linear combination of basis functions, which can be global (harmonics, Zernike polynomials) or local (pixels). In fusion research, plasma emissivity is usually reconstructed by series expansion methods because transformation methods are effective only for regular and dense projections of the reconstructed area, which is not satisfied in tokamaks because of engineering constraints. Furthermore, series expansion methods allow easier implementation of *a priori* information. Series expansion methods are preferably used with local basis functions, in particular, with rectangular pixels, because the alternative approach using global basis functions usually requires a precise knowledge of the plasma center position. In the case of pixel methods, the reconstruction is performed by inversion of the following system of equations:

$$(2) \qquad f_i = \sum_j^N T_{ij} g_j + \zeta_i$$

where f_i is the measured line-integrated radiation, g_j the emissivity associated with the particular pixel, T_{ij} the contribution matrix, N number of pixels, and ζ_i the statistical errors. Value of each element of the contribution matrix T_{ij} (representing influence of the j-th pixel on the i-th detector) can be calculated as a distance which line of sight of i-th detector passes through j-th pixel. This is possible because of the fact that the intensity of a source decreases with squared distance and a collection area of each detector increases with squared distance.

The system of equations is usually highly underdetermined (on COMPASS, number of pixels is typically by two orders of magnitude larger than number of detectors), inversion represents an ill-conditioned
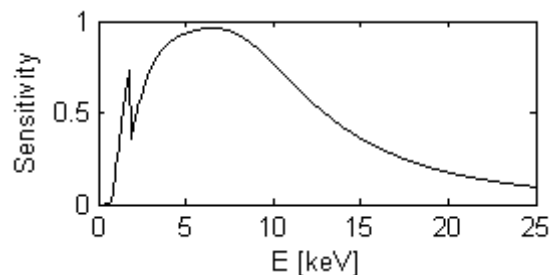

Fig. 3. Theoretical spectral sensitivity of the SXR detectors.

task, and a noise level in the tokamak environment is high. Therefore, regularization algorithms constrained by *a priori* information (e.g., expected smoothness) are often applied to find a unique and reliable solution. Regularization principle is close to the Occam's razor principle. From the infinite number of solutions, the one which is smooth and physically meaningful is chosen. The solution is found by minimizing

$$(3) \qquad \Lambda = \tfrac{1}{2}\chi + \alpha_R R$$

where $\chi^2 = \| (f - T_g)/\sigma_s \|$ is the goodness-of-fit parameter, σ_s the expected data error bars, R regularizing functional, and α_R is the regularization (smoothing) parameter that represents weighting between the goodness of fit and the requirements imposed on the solution g by the functional R.

Minimization ($d\Lambda/dg = 0$) of $\Lambda(g)$ leads to

$$(4) \qquad g(\alpha) = (\mathbf{T^T T} + \alpha \mathbf{H})^{-1} \mathbf{T^T f}$$

where $\mathbf{H}$ contains operators that calculate regularizing functional R from g: $R = \mathbf{g^T H g}$. For example, a smooth solution can be found if R measures 'roughness'. One of the possible choices is the operator of the first derivatives: $H = \nabla_x^T * \nabla_x + \nabla_y^T * \nabla_y = \mathbf{B_x^T B_x} + \mathbf{B_y^T B_y}$, where $\mathbf{B_x}$, $\mathbf{B_y}$ correspond to matrices representing differentiation in horizontal and vertical directions, respectively.

On the COMPASS tokamak, the Fisher information is preferably applied as regularization functional to reconstruct local emissivity. The Fisher information of the probability distribution is defined by $I_F = \int (\nabla g)^2/g \, dS$. In the statistics, the Fisher information is used to measure the amount of information that observable variable carries about the parameter upon which the probability depends. The Fisher information can be used to measure a degree of disorder of the system. In contrast to entropy, the Fisher information includes a local measure (rearrangement of points in the formula for entropy: $S = -\Sigma_j g_j \ln(g_j)$ does not change its value). It is related to variance of the probability distribution σ by the Cramer-Rao inequality:

$$(5) \qquad \sigma^2 \leq 1/I_F$$

Thus, minimization of the Fisher information increases a lower limit of variance of the probability distribution (which is connected with an increase in entropy). In practice, this principle leads to higher smoothness in low emissivity regions. The regularization constrained by minimum Fisher information is complicated by its nonlinearity. However, the system of equations can be linearized by several iterative steps of the weighted linear regularization:

$$(6) \quad g^{(n+1)}(\alpha) = \left(\mathbf{T^T T} + \alpha \left(\mathbf{B_x^T W^{(n)} B_x} + \mathbf{B_y^T W^{(n)} B_y} \right) \right)^{-1}$$
$$\cdot \mathbf{T^T f}$$

where $W^n_{ij} = \delta_{ij}/g^n_i$ for $n > 1$ and $W^1 = 1$ for $n = 1$. This approach was proven to provide robust and reliable solution [3–5].

In plasma tomography, it is beneficial to include magnetic topology because any change in plasma parameters is usually much lower along the magnetic field lines. Equation (6) is then modified into the form:

$$(7) \quad g^{(n+1)}(\alpha) = \left(\mathbf{T^T T} + \alpha \left(\begin{array}{c} \exp(\eta) \mathbf{B_{\|}^T W^{(n)} B_{\|}} \\ + \exp(-\eta) \mathbf{B_{\perp}^T W^{(n)} B_{\perp}} \end{array} \right) \right)^{-1} \cdot \mathbf{T^T f}$$

where $\mathbf{B_{\|}}$, $\mathbf{B_{\perp}}$ correspond to numerical differentiation matrices acting parallel and perpendicular to the magnetic flux surfaces and $\eta > 0$ leads to the preferential smoothing along magnetic field lines.

The regularization task has to implement a suitable choice of the regularization parameter α. One of the methods to determine α is to iteratively change its value so that it matches $\chi^2(\alpha) \to N$, where N is the number of detectors. In the algorithm, the regularization constrained by minimum Fisher information is performed in two nested loops. The outer loop minimizes the Fisher information by solving $g^{(n+1)}(\alpha)$ with $\mathbf{W} = \text{diag}(1/g^{(n)})$ and the inner loop iteratively changes α. Two or three cycles of the outer loop and up to 10 cycles of the inner loop usually lead to the solution with a sufficient convergence (on COMPASS, the condition $|\chi^2(\alpha) - N|/N < 0.05$ is applied).

Differentiation

Tikhonov regularization constrained by minimum Fisher information requires calculating numerical differentiation matrices. There are several ways how to apply numerical differentiation: forward difference, $(g_{k+1} - g_k)/dx$; backward difference, $(g_{k-1} - g_k)/dx$; central difference, $(g_{k+1} - g_{k-1})/2dx$; and higher-order methods. Forward and backward differences are not symmetrical and can lead to artifacts, particularly in case of low resolution. Central difference is symmetrical and approximates the derivative more accurately (error is proportional to dx^2 instead of dx for forward and backward difference), but it is susceptible to $2dx$ oscillations (solution with $2dx$ oscillation can have zero central difference) so it usually results in chessboard-like pattern. Higher-order methods decrease resolution, as they involve more pixels for the calculation of difference at particular pixel. However, the Fisher information calculated by forward or backward difference can be symmetrized by weight matrix $\mathbf{W}$ containing interpolated values of the solution between pixels:

$$(8) \qquad I_F^{\text{forward}} = \sum_k \left(\frac{g_{k+1} - g_k}{dx} \right)^2 \cdot \frac{2}{g_k + g_{k+1}}$$

In general, the weight matrix can be written in the form $w_{ij}^{(n+1)} = \delta_{ij}/(|\mathbf{B}|g^{(n)})_i$. In the case of classical smoothing along vertical and horizontal axis, calculations of the Fisher information by forward differentiation and backward differentiation are equivalent. In the case of preferential smoothing along magnetic field lines, the algorithm finds more precise solution when the Fisher information calculated by forward and backward differentiation are combined:
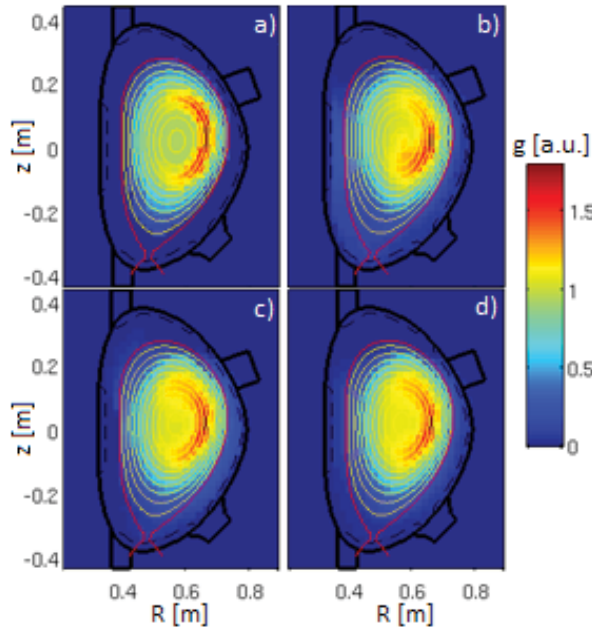
Fig. 4. Model function (a), reconstruction using forward (clockwise) differentiation (b), backward (anticlockwise) differentiation (c), and combination of forward and backward differentiation (d).
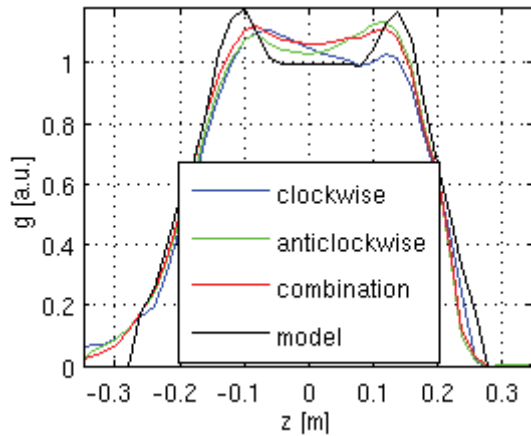
Fig. 5. Vertical profile of the model function and the reconstructions using forward (clockwise) difference, backward difference (anticlockwise), and their combination at $R = 0.56$ m.

$$(9) \qquad I_{\mathrm{F}} = \tfrac{1}{2} I_{\mathrm{F}}^{\mathrm{forward}} + \tfrac{1}{2} I_{\mathrm{F}}^{\mathrm{backward}}$$

As shown in Figs. 4 and 5, applications of different calculations of the Fisher information for reconstruction of phantom function modelling banana profile of emissivity because of the accumulation of impurities and toroidal plasma rotation are compared. Combination of the forward and backward difference led to lower deviation from the model (5%) compared to forward (6.4%) or backward (8.4%) difference. The discrepancy between model agreement for a forward and backward difference is probably caused by different values of the Fisher information in the case of varying direction of differentiation (i.e., in the case of magnetic field lines). In the case of standard differentiation (in vertical and horizontal direction), the Fisher information calcu-

lated by the formula (8) is the same for forward and backward difference (with zero border condition).

Border conditions

Border conditions are particularly important when significant emissivity is to be reconstructed near the border that is usually not the case of SXR tomography. However, it can be worthy to restrict the reconstructed SXR emissivity by border conditions, as they can favourably affect the whole profile. Reconstructed emissivity should be zero outside the tokamak vessel. In order to meet this condition, the algorithm excludes pixels outside the chamber from the calculation and then imposes zero emissivity requirement on chamber's pixels. Exclusion of pixels outside the chamber leads to a faster reconstruction because the computational time increases with the number of pixels (matrix inversion is computed via the Cholesky decomposition whose computational time is proportional to the cubed number of pixels). Requirement of zero emissivity at chamber's pixels can be implemented by two ways: by matrix operator for the Fisher information or by contribution matrix. The former represents smoothing of the edge under the condition of zero values at the chamber, and the later acts as an extension of the detector system by virtual detectors observing zero signals from pixels at the chamber (in the present implementation, each detector sees one pixel at the chamber). Figure 6 compares reconstructed profiles of the model function for different border conditions. In the case of no border conditions, the reconstruction of used model (Gaussian) function led to overestimation of emissivity in the edge of plasma and a higher error in the core. The precision of the reconstruction with border conditions depends on the shape of reconstructed profile. For example, in the case of
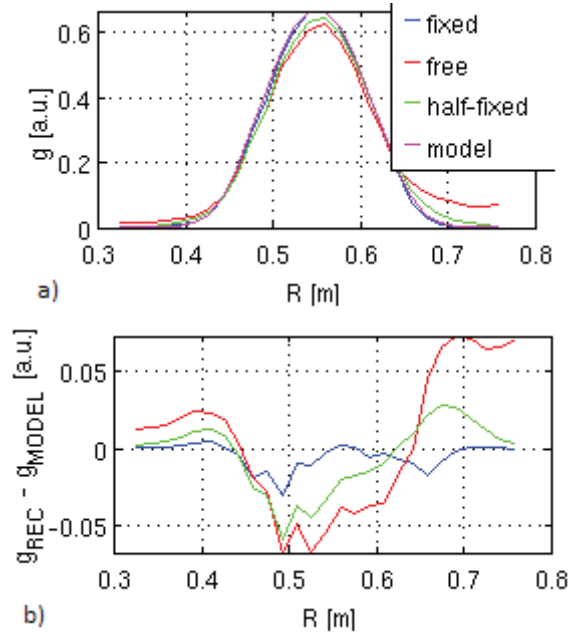
Fig. 6. Profiles reconstructed with different constraint on border conditions for model function $g \sim \exp(-r^3)$ (a) and their differences from the model function (b).
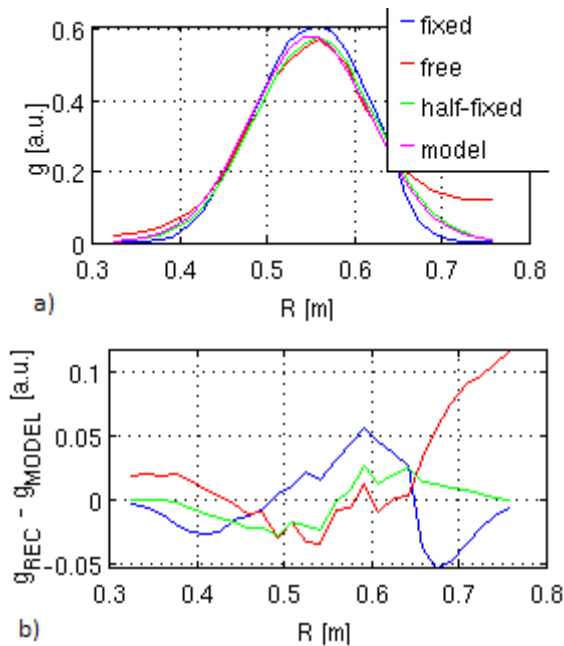
Fig. 7. Profiles reconstructed with different constraint on border conditions for model function $g \sim \exp(-r^2)$ (a) and their differences from the model function (b).

model function shown in Fig. 7a ($g \sim \exp(-r^3)$ where r represents the distance from the center), the most accurate reconstruction uses 'half-fixed' borders, that is, reconstruction with lower weight (lower values representing border condition in the matrix operator) of border conditions on the solution. As the SXR profile measured in the COMPASS tokamak

is usually highly peaked and located in the plasma center, the fixed border conditions are applied.

Rolling iteration

The plasma radiation profile can be assumed to be evolving smoothly during most phases of the discharge. Using this assumption, the iteration can be accelerated by using the results from the last time frame as initial guesses for the current frame (both the values of α and g). Alternatively, this may be viewed as doing the iteration continuously while changing the input data at certain moments (denoted as rolling iteration). The result is returned at the same time.

An extreme form of the rolling iteration is changing the data in every iteration step. In this case, the iteration is left no time to converge when the initial guess is inaccurate. The quality of the solution depends on the assumption of smooth plasma evolution. However, the long-term stability of the method remains good. In the case of a sudden change in the emissivity profile, it typically takes several frames for the method to approach the correct solution again. The convergence rate differs for various quantities estimated from the reconstructions. For example, the error of plasma position seems to decay exponentially with a time constant of 3–4 frames. In contrast, the changes in total radiated power are reconstructed instantly [6].

For the tomographic algorithms with linear regularization functional, the rolling iteration reduces to
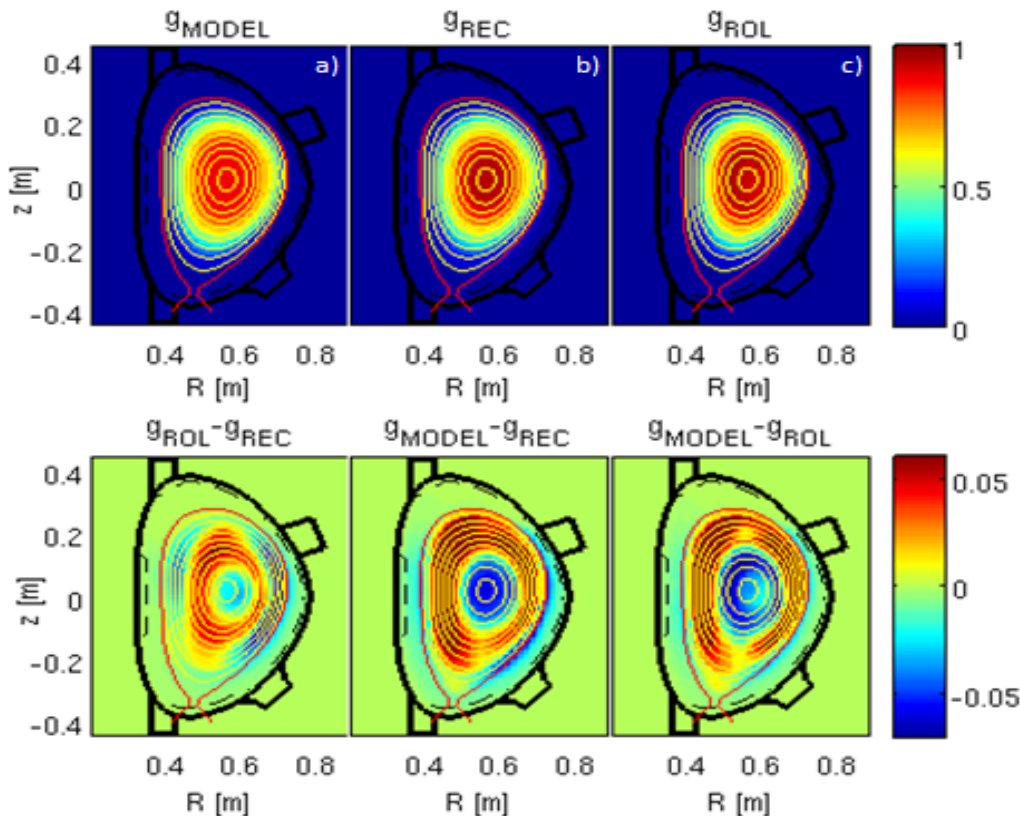
Fig. 8. Model function g_{model} (a), its tomographic reconstruction g_{REC} (b), reconstruction by the rolling iteration g_{ROL} (c) just after a modelled sawtooth crash (sudden flattening of the profile), and their differences.

a fast and less accurate way to estimate α. However, there is a possibility to exploit the knowledge of previous result more. The system of linear equations can be solved using an iterative method, which needs an initial approximation. The previous result may be used as this approximation, which may reduce the number of iterations that is needed to reach the required accuracy. This approach is currently under development on COMPASS.

Figure 8 shows phantom function modelling sawtooth oscillations just after the sawtooth crash (sudden flattening of the profile) and its tomographic reconstruction by standard algorithm and rolling iteration. The differences between the model function and both reconstructions show an overestimation of emissivity in the center, which is a typical behaviour of the Tikhonov regularization constrained by minimum Fisher information in the case of profiles with low peakedness [7]. The difference between the standard algorithm and the rolling iteration is lower (up to 5%) than the difference between reconstructions and model function, suggesting reliability of the rolling iteration for sudden changes in the emissivity profile.

Summary

The contribution deals with optimization of the Tikhonov regularization constrained by minimum Fisher information for SXR tomography by means of symmetrization of calculation of the Fisher information, choice of border conditions, and adaptation of the algorithm for real-time tomography. Symmetrization of the Fisher information was shown to suppress the artifacts that can occur in reconstructed emissivity. Border conditions in the form of the exclusion of pixels outside the chamber and requirement of zero emissivity at chamber's pixels led to faster reconstruction with a more reliable solution. In the case of fast changes in plasma emissivity, the algorithm for real-time tomography typically needs several frames to approach the correct solution, but it still provides a reliable solution as the discrepancy between the real-time and standard algorithm is not high (below 10%).

References

1. Panek, R., Bilková, P., Fuchs, V., Hron, M., Chraska, P., Stockel, J., Urban, J., Weinzettl, V., Zajac, J., & Zacek, F. (2006). Reinstallation of the COMPASS-D tokamak in IPP ASCR. *Czech. J. Phys.*, *56*(Suppl. 2), B125–B137. DOI: 10.1007/s10582-006-0188-1.
2. Weinzettl, V., Naydenkova, D. I., Sestak, D., Vlcek, J., Mlynar, J., Melich, R., Jares, D., Malot, J., Sarychev, D., & Igochine, V. (2010). Design of multi-range tomographic system for transport studies in tokamak plasmas. *Nucl. Instrum. Methods Phys. Res. Sect. A-Accel. Spectrom. Dect. Assoc. Equip.*, *623*, 806–808. DOI: 10.1016/j.nima.2010.04.010.
3. Anton, M., Weisen, H., Dutch, M. J., Linden, W., Buhlmann, F., Chavan, R., Marletaz, B., Marmillod, P., & Paris, P. (1996). X-ray tomography on the TCV tokamak. *Plasma Phys. Control. Fusion*, *38*, 1849–1878. DOI: 10.1088/0741-3335/38/11/001.
4. Odstrcil, M., Mlynar, J., Odstrcil, T., Alper, B., Murari, A., & JET EFDA Contributors. (2012). Modern numerical methods for plasma tomography optimization. *Nucl. Instrum. Methods Phys. Res. Sect. A-Accel. Spectrom. Dect. Assoc. Equip.*, *686*, 156–161.
5. Mazon, D., Vezinet, D., Pacella, D., Moreau, D., Gabelieri, L., Romano, A., Malard, P., Mlynar, J., Masset, R., & Lotte, P. (2012). Soft x-ray tomography for real-time applications: present status at Tore Supra and possible future developments. *Rev. Sci. Instrum.*, *83*(6), 063505. DOI: 10.1063/1.4730044.
6. Loffelmann, V., Mlynar, J., Imrisek, M., Mazon, D., Jardin, A., Weinzettl, V., & Hron, M. (2016). Minimum Fisher Tikhonov regularization adapted to real-time tomography. *Fusion Sci. Technol.*, *69*(2), 505–513.
7. Ingesson, L. C., Alper, B., Peterson, B. J., & Vallet, J.-C. (2008). Tomography diagnostics: Bolometry and soft X-ray detection. *Fusion Sci. Technol.*, *53*(2), 528–576.

A.3 Attached article: Use of soft x-ray diagnostic on the COMPASS tokamak for investigations of sawteeth crash neighborhood and of plasma position using fast inversion methods

Use of soft x-ray diagnostic on the COMPASS tokamak for investigations of sawteeth crash neighborhood and of plasma position using fast inversion methods[a)]

M. Imrisek,[1,2] V. Weinzettl,[1] J. Mlynar,[1] T. Odstrcil,[3] M. Odstrcil,[4,5] O. Ficker,[4] J. R. Pinzon,[6]
C. Ehrlacher,[7] R. Panek,[1] and M. Hron[1]

[1]*Institute of Plasma Physics ASCR, Prague, Czech Republic*
[2]*Faculty of Mathematics and Physics, Charles University in Prague, Prague, Czech Republic*
[3]*Max-Planck-Institut für Plasmaphysik, Garching, Germany*
[4]*Faculty of Nuclear Sciences and Physical Engineering, Czech Technical University in Prague,
Prague, Czech Republic*
[5]*Optical Research Center, University of Southampton, Southampton, United Kingdom*
[6]*Institue Jean Lamour, Université de Lorraine, Nancy, France*
[7]*ENS Cachan, Paris, France*

The soft x-ray diagnostic is suitable for monitoring plasma activity in the tokamak core, e.g., sawtooth instability. Moreover, spatially resolved measurements can provide information about plasma position and shape, which can supplement magnetic measurements. In this contribution, fast algorithms with the potential for a real-time use are tested on the data from the COMPASS tokamak. In addition, the soft x-ray data are compared with data from other diagnostics in order to discuss possible connection between sawtooth instability on one side and the transition to higher confinement mode, edge localized modes and productions of runaway electrons on the other side.
[http://dx.doi.org/10.1063/1.4894528]

I. SOFT X-RAY DIAGNOSTIC ON THE COMPASS TOKAMAK

In tokamak plasmas without heavy impurities, the soft x-ray (SXR) radiation is generated mainly by bremsstrahlung which depends on both electron density n_e and temperature T_e:

$$P_{brem} \sim Z_{eff} n_e^2 \sqrt{T_e}, \quad (1)$$

where $Z_{eff} = \sum_i n_i Z_i^2 / n_e$ is effective ion charge, and n_i is density of Z_i-times charged ions. Since the temperature profile is usually peaked in the plasma core and density can have flat as well as peaked profile, the SXR diagnostic is suitable for monitoring plasma core activity, e.g., the sawtooth instability. Moreover, spatially resolved measurements can provide information about plasma position and shape. Measured signals always correspond to chord integrated soft x-ray radiation, therefore, inversion methods (tomography), which are reviewed in Sec. II, have to be applied in order to obtain spatial distribution of the plasma emissivity.

The COMPASS tokamak, a divertor device with clear H-mode and ITER-relevant geometry (1:10 to ITER plasma size, $R = 0.56$ m, $a = 0.23$ m, $Ip < 400$ kA, $B_T \sim 1.15$ T and typical pulse length around 300 ms)[1] is equipped with the fast SXR diagnostic system[2] based on silicon photodiode arrays shielded by the beryllium foil. The diagnostic is composed of two pinhole cameras having 35 channels each (Centronic,

type LD35-5T) and one vertical pinhole camera with 20 channels which has been installed recently (IRD, type AXUV-20EL) (see Fig. 1) to improve tomographic inversions. Spatial resolution of each camera is about 1–2 cm. Temporal resolution of the SXR diagnostic is constrained mainly by the amplifier to about 3 μs allowing an investigation of fast magneto-hydrodynamic processes and instabilities in the plasma core. The spectral sensitivity of the system is mainly determined by thickness of beryllium foil (10 μm) filtering out photons with energy below 1 keV and by thickness of diode active layer[3] (about 200 μm) which limits the detector sensitivity to photon energies below 13 keV.

II. INVERSION METHODS

Local emissivity can be estimated by inversion methods for a discrete set of rectangular pixels, so that the relationship between the line integrated data f_i and emissivity distribution g_j can be written as[3]

$$f_i = \sum_j^N T_{ij} g_j + \zeta_i, \quad (2)$$

where T_{ij} is the contribution matrix, N number of pixels, and ζ_i statistical errors. However, tokamak plasma projections are sparse due to the engineering constraints and, moreover, the inversion represents an ill-conditioned task. In order to find a unique solution, regularization algorithms constrained by *a priori* information (e.g., expected smoothness) are used. A unique solution can be found by minimizing

$$\Lambda = \frac{1}{2}\chi^2 + \alpha F(g), \quad (3)$$
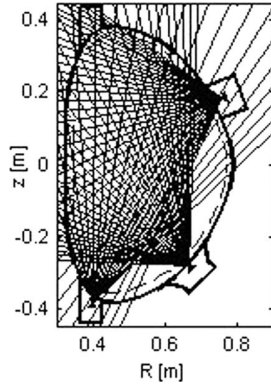
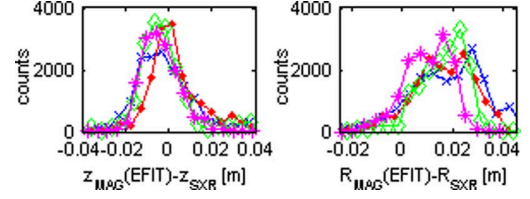FIG. 1. Geometry of SXR detectors on the COMPASS tokamak.

FIG. 2. Histogram of vertical (left) and horizontal (right) differences between magnetic axis (reconstructed by EFIT) and the center of mass of SXR radiation obtained by full tomographic reconstruction (MFR denoted by magenta stars) comparing fast methods based on precomputing weight vectors using SVD (blue x-marks), QR (red dots), GEV (green diamonds). Data were obtained from 90 various discharges with a typical D-shaped configuration.

where χ^2 is the goodness-of-fit parameter, α is the regularization (smoothing) parameter, and F is the regularization functional. Minimum Fisher regularization[4] (MFR) is often applied to find a smooth solution by choosing the Fisher information as the regularization functional. MFR has proved to find robust and reliable solution.[5] Weighted anisotropic derivatives with respect to the magnetic flux surfaces in the Fisher information allow finding a solution with higher smoothness along magnetic field lines.

Among other parameters, tomographic reconstruction can be used to evaluate the center of mass of the SXR emission related to the plasma position. This could be used to supplement magnetic measurements of plasma position, which may suffer from integration drifts during long shots. However, standard tomography reconstruction of plasma profile is inconvenient for real-time calculations. Simplified linear methods allow faster reconstruction in exchange for lower precision. Their main advantage is the possibility to precalculate a decomposition of the emissivity distribution into global basis functions (depending only on the geometry of experiment). Then, these methods can be used for calculation of weight vectors for distribution moments. In the linear methods used in this contribution, the regularization is constrained by the smoothness of solution, i.e., $F(g) = \|\mathbf{C}g\|^2$, where $\mathbf{C}$ is numerical differentiation matrix. During the minimization of Eq. (3), the decomposition $\mathbf{TC}^{-1} = \mathbf{U\Sigma V}^T$ by SVD[6] (Singular Value Decomposition), QR[7] based method, or GEV[8] (Generalized Eigen Values) based method leads after several steps to a solution in the form

$$g(\alpha) = \sum_j w_j(\alpha) \frac{f \cdot u_j}{\sigma_j} C^{-1} v_j, \qquad (4)$$

where u_j and v_j are columns of $\mathbf{U}$ and $\mathbf{V}$, σ_j diagonal elements of singular values $\mathbf{\Sigma}$, and $w_j(\alpha) = (1 + \alpha/\sigma_j^2)^{-1}$ can be seen as a low-pass filter which cuts off components with higher j as σ_j decreases. It is observed that the optimal value of α can be chosen as med ($\mathbf{\Sigma}$). This approach is independent of measured data (in contrast to the generalized cross-validation[5] or finding the roots of $\chi^2 = 1$). The center of mass of SXR radiation can be then derived from Eq. (4) as a scalar multiplication of measured data with precomputed weight vectors for the first moments b_{1r}, b_{1z} normalized by scalar multiplication of mea-

sured data with the zeroth moment b_0:

$$[r_{ctr}, z_{ctr}] = \left[\frac{b_{1r} \cdot f}{b_0 \cdot f}, \frac{b_{1z} \cdot f}{b_0 \cdot f} \right]. \qquad (5)$$

Furthermore, higher moments providing information about plasma shape can be obtained in a similar way. Scalar multiplication of measured data by weight vectors is faster (several μs) than sophisticated tomographic methods like MFR (hundreds of ms) which is a crucial advantage for the real-time plasma position control. Weight vectors calculated by different matrix decomposition techniques as SVD, QR, or GEV are used to obtain the center of mass of SXR radiation. The results are comparable with the MFR-based tomography (see Fig. 2). The GEV method provides results with lower standard deviations of difference between magnetic and SXR-based positions (1.2 cm for horizontal and 1.6 cm for vertical direction) than the QR and the SVD method. This root-mean-square-deviation is comparable to the spatial resolution of the SXR detectors. The average horizontal SXR positions are positioned closer to the high field side as a result of Shafranov shift and SXR profile is affected by plasma configuration.

III. STUDIES OF SAWTOOTH INSTABILITY

The sawtooth oscillation is one of the fundamental instabilities occurring in the plasma core. Repetitive slow increase and fast drop in both the core temperature and density can be seen as sawtooth pattern on several signals, including in particular SXR.[9] The sawtooth instability is an important topic in the fusion research, because it affects the hottest part of the plasma volume, and triggers other instabilities below their threshold.[9] On the other hand, it can help to
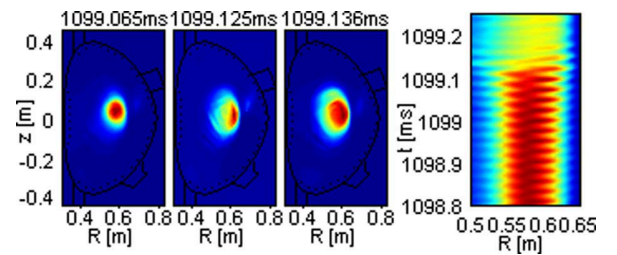

FIG. 3. Left: Reconstructed SXR emissivity just before, in the moment, and just after the sawtooth crash. Right: A time evolution of reconstructed radial profile of SXR emissivity showing the internal kink mode accompanying the sawtooth crash in shot 6071.
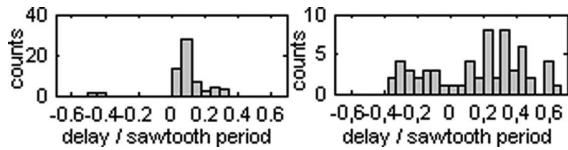
FIG. 4. The delay of the L-H (left) and H-L (right) transitions after the sawtooth crash.

FIG. 6. ELM distribution with respect to the time of the sawtooth crash measured in 82 shots (left) and observed coupling of ELMs with sawtooth crashes in shot 5909 (right).

remove helium ash from the plasma core. The sawtooth crash is usually accompanied by precursor oscillations which corresponds to the internal kink mode m = n = 1. Kadomtsev model[10] provides a starting point for an understanding of the sawtooth crash, however, it is in contradiction with several measurements.[11,12] Presently, a partial reconnection model[13] is often preferred for the interpretation of the sawtooth crash. For example, oscillations of the hot core in reconstructed radial profile (see Fig. 3) show that the mode position remains unchanged after the crash which is in contradiction with the Kadomtsev model. However, absence of the post-crash oscillations violating the partial reconnection model is also observed.

The sawtooth crash can trigger the L-H transition.[14] It is supposed that the hot plasma expelled from the central region to the edge can supply enough free energy to the formation of the edge transport barrier. The synchronization of the L-H transition with the sawtooth crash is very clear at the COMPASS tokamak as it can be seen in Fig. 4 left. In contrast to this observation, there is no clear evidence of synchronization of the sawtooth crash with the H-L transition (see Fig. 4 right).

During the sawtooth crash, hard X-ray radiation (HXR) has been often detected on COMPASS (see Fig. 5). HXR is usually observed in low density plasmas and during disruptions as a consequence of runaway electrons generation due to low collisionality and strong toroidal electric field. A possible mechanism of the electron acceleration during the sawtooth crash proposed by Klimanov[15] suggests that runaway electrons are driven by magnetic reconnection. However, no significant relation between the amplitude of sawteeth and HXR intensity caused by runaway electrons was observed on the COMPASS tokamak.

On rare occasions, sawtooth crashes are observed to tightly precede edge localized modes (ELM), see Fig. 6 left. Although Nave[16] observed larger sawteeth crashes coupling with ELMs, on COMPASS not focusing at any particular plasma parameter, synchronisation of the ELMs and sawtooth crashes is not related to the amplitude of the sawtooth instability. A possible correlation between ELM and sawtooth instabilities is indicated by a drop in ELM distribution about 0.5 ms after the sawtooth crash. This observation can be possibly explained in terms of improved plasma stability in the sawtooth ramp phase. More extensive statistics is necessary for proper evaluation of this effect.

IV. DISCUSSION AND SUMMARY

Fast algorithms for calculation of the center of SXR radiation have been successfully applied on data from the COMPASS tokamak. In further applications, it is to be noted that this value can be affected by asymmetry in density profile of the heavy impurities (in particular in tokamaks with tungsten divertor), which would require corrections for centrifugal force and other influences. Information on poloidal asymmetry can be partly provided by higher moments. Nevertheless, the linear methods allow fast calculation of the distribution moments which are more convenient for real-time use. Limitations, possible corrections, and a potential of fast algorithms for real-time use are to be further examined. Furthermore, the SXR data were used to investigate the plasma core activity during the sawtooth crash. Next, the SXR emissivity was compared with other diagnostics to show clear triggering of the L-H transition by the sawtooth crash and to discuss the influence of the sawtooth instability on the ELMs and on the runaway electrons. More data and further studies, e.g., concerning the role of inversion radius in the sawteeth instability as obtained from SXR tomography[3] and/or the amplitude of instability could further clarify possible influence of the sawtooth instability on the L-H transition, ELMs, and runaway electrons.
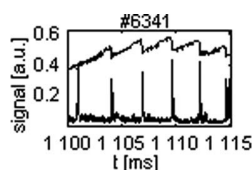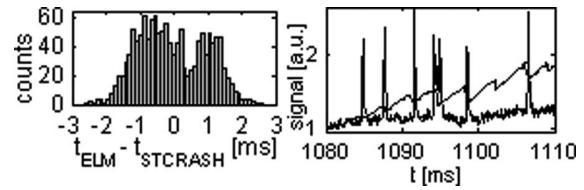
ACKNOWLEDGMENTS

FIG. 5. Typical SXR signals (upper line) during the sawtooth instability and measured HXR radiation (lower line). The HXR peaks indicate interaction between runaway electrons and the vessel.

[1] R. Panek, P. Bilková, V. Fuchs, M. Hron, P. Chraska, P. Pavlo, J. Stockel, J. Urban, V. Weinzettl, J. Zajac, and F. Zacek, Czechoslovak J. Phys. **56**(2), B125–B137 (2006).
[2] V. Weinzettl, D. I. Naydenkova, D. Sestak, J. Vlcek, J. Mlynar, R. Melich, D. Jares, J. Malot, D. Sarychev, and V. Igochine, Nucl. Instrum. Methods Phys. Res. A **623**, 806–808 (2010).
[3] V. Igochine, A. Gude, M. Maraschek, and ASDEX Upgrade team, Internal IPP report 1/338, 2010.
[4] M. Anton, H. Weisen, M. J. Dutch, W. Linden, F. Buhlmann, R. Chavan, B. Marletaz, P. Marmillod, and P. Paris, Plasma Phys. Controll. Fusion **38**, 1849 (1996).

[5]J. Mlynar, M. Imrisek, V. Weinzettl, M. Odstrcil, J. Havlicek *et al.*, Rev. Sci. Instrum. **83**, 10E531 (2012).

[6]N. Terasaki, Y. Hosoda, M. Teranishi, and N. Iwama, Fusion Eng. Des. **34-35**, 801–804 (1997).

[7]Y. Hosoda and T. Torii, Jpn. J. Appl. Math. **4**, 287–298 (1994).

[8]G. C. Fehmersy, L. P. J. Kamp, and F. W. Sluijter, Inverse Problems **14**, 893–901 (1998).

[9]I. T. Chapman *et al.*, Plasma Phys. Controll. Fusion **53**, 013001 (2011).

[10]B. B. Kadomtsev, Sov. J. Plasma Phys. **1**, 389 (1976).

[11]J. Blum, E. Lazzaro, J. O'Rourke, B. Keegan, and Y. Stephan, Nucl. Fusion **30**,1475 (1990).

[12]A. W. Edwards *et al.*, Phys. Rev. Lett. **57**, 210 (1986).

[13]F. Porcelli, D. Boucher, and M. Rosenbluth, Plasma Phys. Controll. Fusion **38**, 2163 (1996).

[14]Y. R. Martin and TCV team, Plasma Phys. Controll. Fusion **46**, A77–A85 (2004).

[15]I. Klimanov, A. Fasoli, T. P. Goodman, and the TCV team, Plasma Phys. Control. Fusion **49**, L1–L6 (2007).

[16]M. F. F. Nave *et al.*, Nucl. Fusion **35**, 409 (1995).